Supporting Information

Boosting Electrochemical Water Oxidation Reaction of Hierarchical Nanoarrays through NiFe-oxides/Ag Heterointerfaces

Bin Zhu[#], Qi Hu[#], Xiufang Liu, Guomin Li, Liangdong Fan, Qianling Zhang, Jianhong Liu and Chuanxin He*

Department of Chemistry, College of Chemistry and Environmental Engineering, Shenzhen University, Shenzhen, Guangdong, 518060, China

** Corresponding Author: Prof. Chuan-Xin He (Tel: +86 0755-26536141, E-mail:hecx@szu.edu.cn).*

Experimental section

1.1 Electrocatalysts synthesis

1.1.1 Chemicals and materials

Nickel nitrate hexahydrate ($Ni(NO_3)_2.6H_2O$), Ferric nitrate nonahydrate ($Fe(NO_3)_3.9H_2O$), ammonium fluoride (NH_4F), Sodium hydroxide (NaOH), and Sodium carbonate anhydrous (Na_2CO_3) were purchased from Aladdin Co., Ltd. The commercial ruthenium (IV) oxide (RuO_2) was purchased from Alfa Aesar Co., Ltd. The carbon paper (CP) was purchased from Shanghai Hesen Electric Co., Ltd. Silver nanowires were synthesized from our laboratory. All the chemicals were of analytical grade and used directly without any further purification after purchasing. Deionized

water was purified by a Milli-Q system.

1.1.2 Synthesis of Silver Nanowires (Ag NWs)

One-dimensional (1D) Ag NWs were prepared based on the previous literature [1]. In a typic process, PVP (0.5 g) was dispersed into 30 mL of ethylene glycol (EG) at room temperature to form a PVP-EG mixed solution under magnetic stirring. And then, $AgNO_3$ (0.3 g) and $FeCl_3$ (3 g) were dissolved into the above PVP-EG solution to generate a clear solution, which was then heated to 130 ℃ for 10 h. Finally, the resulting Ag NWs were washed with ethanol and deionized water each for three times and then dispersed in deionized water to form Ag NWs suspension with concentration of 9 mg ml^{-1} for further use.

1.1.3 Synthesis of the NiFe-oxides (denoted NiFe-O) nanosheet arrays grown on Ag NWs (denoted NiFe-O/Ag)

Above as-synthesized Ag NWs suspension (1.7 ml containing 15 mg Ag NWs) was dispersed in 250 mL of mixed metal salts solution containing $Ni(NO_3)_2 \cdot 6H_2O$ (0.066 mol), $Fe(NO_3)_3.9H_2O$ (0.033 mol), and NH_4F (0.048 mol) by ultra-sonication for 60 min. A second solution (70 ml) containing NaOH (0.14 mol) and Na_2CO_3 (0.36 mol) was then added dropwise into the above solution under vigorous stirring and aged at room temperature for 13 h. The resulting suspension was washed thoroughly with deionized water until pH 7.0, and then dried at room temperature. The obtained product was denoted NiFe-LDH/Ag. Finally, the NiFe-LDH/Ag was calcined at 300 ^oC for 2 h under Ar atmosphere, and the calcined product was denoted NiFe-O/Ag. The NiFe-O sample without Ag NWs was synthesized as the same procedure as that

of NiFe-O/Ag except adding Ag NWs. For comparison, the NiFe-oxides nanosheet arrays were also grown on the carbon nanotubes (CNT) through the same procedure as that of NiFe-O/Ag but changing the Ag NWs to CNT. The adding amount of CNT was 15 mg. The resulting product was denoted NiFe-O/CNT. The NiFe-O-1/Ag and NiFe-O-3/Ag (1 and 3 refer to the molar ratio of Ni^{2+} to Fe^{3+} ions) were also prepared as controlled samples through the same precure of NiFe-O/Ag except that the molar ratio of Ni^{2+} to Fe^{3+} ions changed to 1 and 3, respectively. The total amount of Ni^{2+} and Fe^{3+} (0.099 mol) were same as that of NiFe-O/Ag

1.2 Material Characterization.

The morphology characterization of as-synthesized samples was conducted on field emission scanning electron microscopy (FESEM, JSM-7800F, Japan) and transmission electron microscopy (TEM, JEM-2100, Japan). High-resolution TEM (HRTEM), Energy Dispersive X-Ray Spectroscopy (EDX) and EDX mapping were collected on JEM-2100F. XRD data was collected on a D8ADVANCE diffractometer with graphite-filtered CuKα source (λ = 1.54056 Å) over a range of 20^{o} to 70^{o}. X-ray photoelectron spectroscopy (XPS) measurements were performed on a Thermo VG ESCALAB250 X-ray photoelectron spectrometer with AlKα X-ray radiation.

1.3 Electrocatalysis test

Electrochemical measurements were carried on an electrochemical workstation (CHI 600C) using a typical three-electrode system in 1 M KOH solution saturated with O_2 gas. Carbon paper served as the substrate for the working electrode (geometric surface area: 1.00 cm^2). A Pt foil and Hg/HgO electrode were used as the

counter electrode and the reference electrode, respectively. The measured potential values vs. the Hg/HgO were converted into those vs. the RHE according to the Nernst equation: E(RHE)= E (Hg/HgO) +0.931V. To prepare the working electrode, the as-synthesized catalysts (0.826 mg) was firstly dispersed mixed solution of ethanol (95 μL), deionized water (300 μL), and Nafion (18 μL) under condition of sonication for at least 30 min to form a homogeneous electrocatalyst inks. Afterward, the above catalyst ink (143 μL) was drop-casted on the carbon paper electrode (mass loading: ~0.286 mg cm^{-2}) and dried at room temperature. All the measurements were performed in 1 M KOH electrolyte solution saturated with O_2 gas. To activate as-synthesized electrocatalysts, five initial cycles of cyclic voltammetry scans (1.2-1.8 V vs RHE) were performed on the catalysts. Afterwards, the linear sweep voltammetric (LSV) curves were collected at a scan rate of 2 mV s^{-1} over a potential range of 1.1 to 1.8 V vs RHE. All the LSV were IR-corrected using a measurement of single-point high-frequency impedance, and the corrected resistance was tested in value of 21 Ω in 1 M KOH. The electrochemical impedance spectroscopy (EIS) was tested from 1 MHz to 1 Hz at the overpotential of 300 mV in 1 M KOH solution. The long-time stability of NiFe-O/Ag sample for OER was measured by the chronoamperometry at overpotential of 400 mV.

1.4 Electrical Double Layered Capacitance measurement

Normally, the electrochemically active surface area (ECSA) can be calculated on the basis of double layer capacitance (C_{dl}). To determine C_{dl} of various electrocatalysts, cyclic voltammograms at different scan rates (i.e., 0.04, 0.06, 0.08,

0.10, 0.12 and 0.14 V/s) were conducted over electrocatalysts over a non-Faradic potential range of 1.15 to 1.25 V vs RHE. The capacitive current was then plotted at 1.20 V against cyclic voltammograms scan rates, and the slope of the fitted line can be considered as twice C_{dl}. Finally, the ECSA was calculated by the following equation:

$$ECSA = \frac{C_{\mathrm{dl}}}{C_{\mathrm{s}}}$$

where C_s is the specific capacitance of an atomically smooth surface of material under identical electrochemical condition. The common specific capacitance of C_s = 0.04 mF cm^{-2} was used in the estimate.[2]

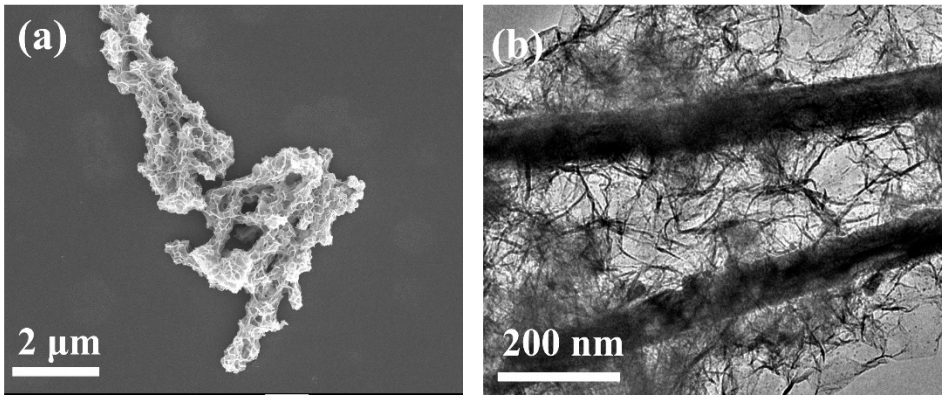

Fig. S1 (a) SEM images and (b) TEM images of NiFe-layered double hydroxides supported on Ag NWs (denoted NiFe-LDH/Ag)

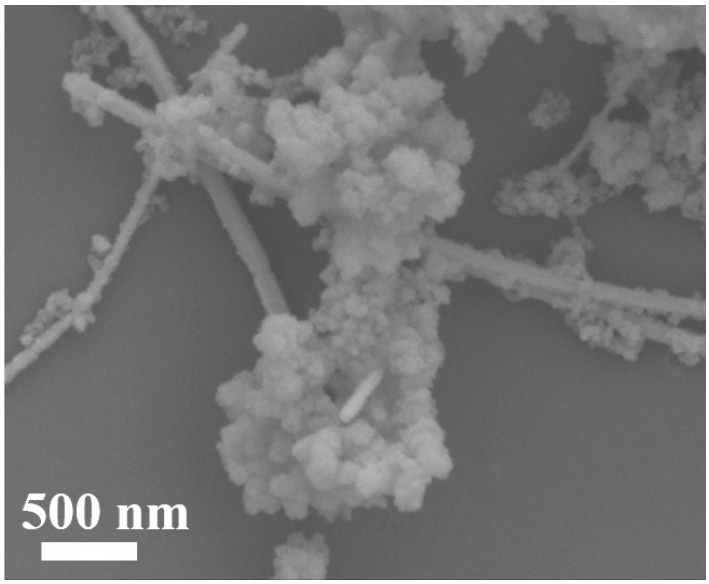

Fig. S2 SEM images of NiFe-LDH/Ag sample, which is prepared via a coprecipitation with a fast speed of adding mixed alkaline solution.

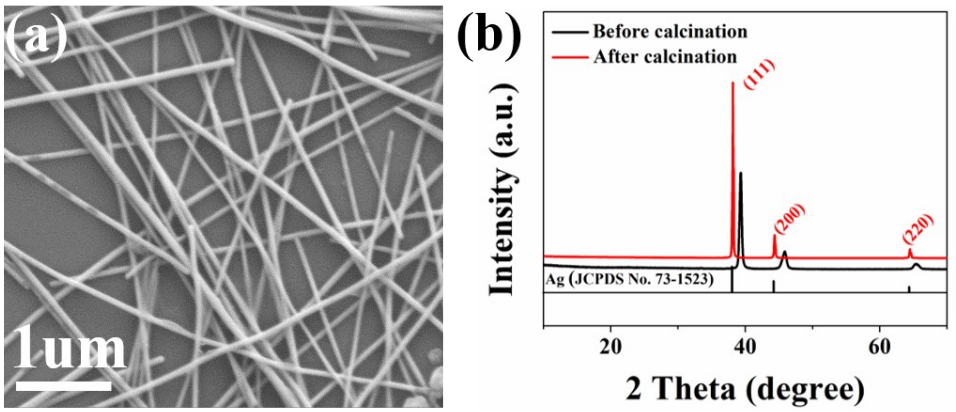

Fig. S3 (a) SEM images and (b) typical XRD patterns of as-synthesized Ag NWs.

As shown in Fig. S3, the as-synthesized Ag NWs are in diameter of ~60 nm and in length of ~5 μm. Interestingly, the XRD peaks of pristine Ag NWs are shifted to higher 2θ angles of ~1° as compared to the standard peaks of metallic Ag (JCPDS No. 73-1523). Notably, in the synthesis of Ag NWs, abundant polyvinylpyrrolidone (PVP) was added as growth regulator. Therefore, there should be PVP coated on the as-synthesized Ag NWs. In this context, we removed the PVP from Ag NWs through calcination at 300 °C for 2 h under Ar atmosphere. After removing PVP, the XRD peaks of Ag NWs are shifted to lower 2θ angles of ~1°, and in well accordance with the standard peaks of metallic Ag. The above results suggest that the 2θ angles shift on XRD pattern of pristine Ag NWs (i.e. before calcination) is resulted from the presence of PVP on the surface of Ag NWs.

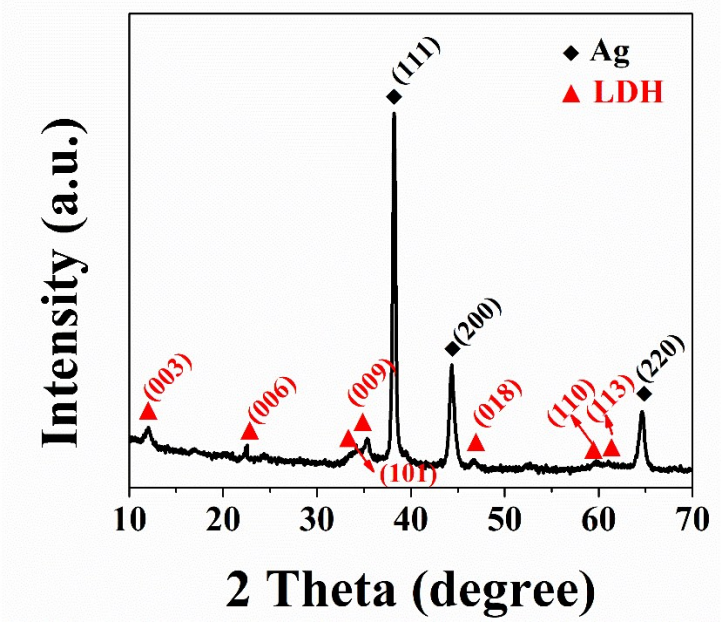

Fig. S4 The XRD pattern of NiFe-layered double hydroxides (NiFe-LDH) nanosheet arrays grown on Ag NWs (denoted NiFe-LDH/Ag).

The XRD pattern of NiFe-LDH/Ag sample display distinct peaks at 2θ of 38.2, 44.4 and 64.6°, corresponding to (111), (200), and (220) plane of metallic Ag, respectively. (Fig. S4) Moreover, the XRD peaks at 2θ of 11.8, 22.3, 34.1, 35.2, 46.2, 60.0 and 61.1°, which can be indexed in to (003), (006), (101), (009), (018), (110) and (113) plane of NiFe-LDH (JCPDS No. 37-0630).[3] The above results signify the formation of nanocomposites composed of NiFe-LDH and Ag NWs.

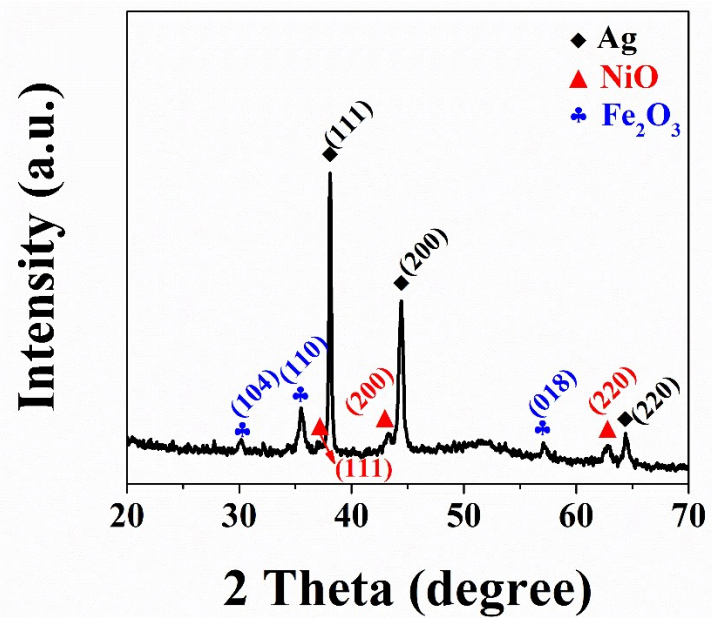

Fig. S5 The XRD pattern of NiFe-oxides (NiFe-O) nanosheet arrays supported on Ag NWs (NiFe-O/Ag). The NiFe-O/Ag was synthesized via one-step calcination of NiFe-LDH/Ag.

As shown in Fig. S5, the XRD peaks at 2θ of 37.1, 43.3, and 62.9°, corresponding to (104), (110), and (018) plane of NiO (JCPDS No. 73-1523). The XRD peaks at 2θ of 30.2, 35.5, and 57.1° can be attributed to the (104), (110), and (018) plane of Fe_2O_3 (JCPDS No. 89-0597). The other three distinct peaks at 2θ of 38.2, 44.4 and 64.6° are considered as (111), (200), and (220) plane of Ag NWs. Clearly, the XRD results suggest the presence of both mixed NiFe-oxides and Ag NWs on NiFe-O/Ag sample.

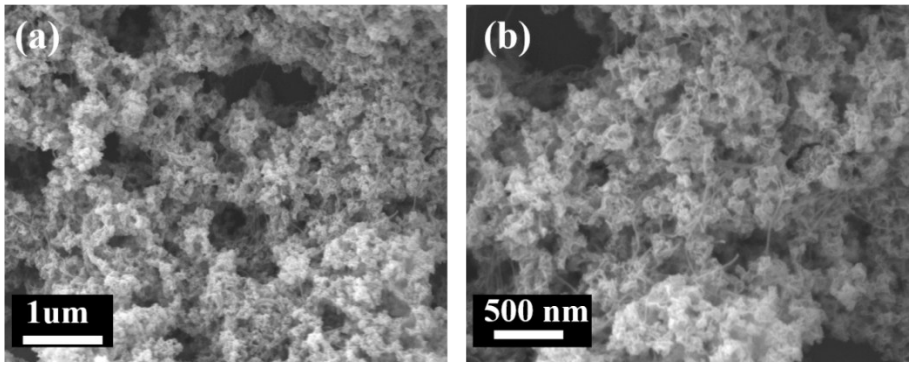

Fig. S6 SEM images of NiFe-oxides (NiFe-O) nanosheet arrays supported on carbon nanotubes (CNT) (denoted NiFe-O/CNT, served as control sample).

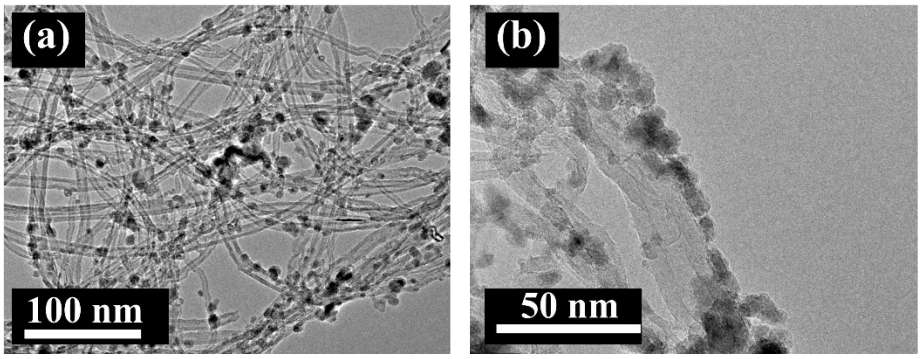

Fig. S7 TEM images of NiFe-O/CNT.

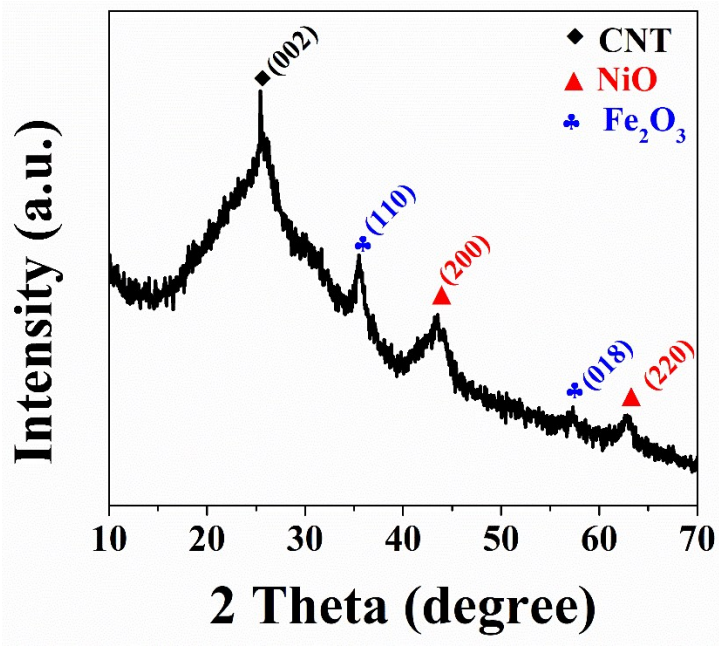

Fig. S8 XRD patterns of NiFe-O/CNT.

The Fig. S6 shows the typic SEM images of NiFe-O/CNT, indicating the presence of small NiFe-oxides nanosheets on the surface of carbon nanotubes (CNT). (Fig. S6) Furthermore, the TEM images manifest that the NiFe-oxides nanosheets are in diameter of ~10 nm. (Fig. S7) The XRD pattern of NiFe-O/CNT shows an obvious peak of (002) plane for graphitic carbon at 2θ of 25.4°, along with peaks at 2θ of 43.6 and 62.9° corresponding to (200) and (220) plane of NiO (JCPDS No. 73-1523). (Fig. S8) The XRD peaks at 2θ of 35.5 and 57.2° can be indexed into (110) and (018) plane of Fe_2O_3 (JCPDS No. 89-0597). The above results undoubtedly suggest the presence of NiFe-oxides nanosheets coated on the surface of carbon nanotubes.

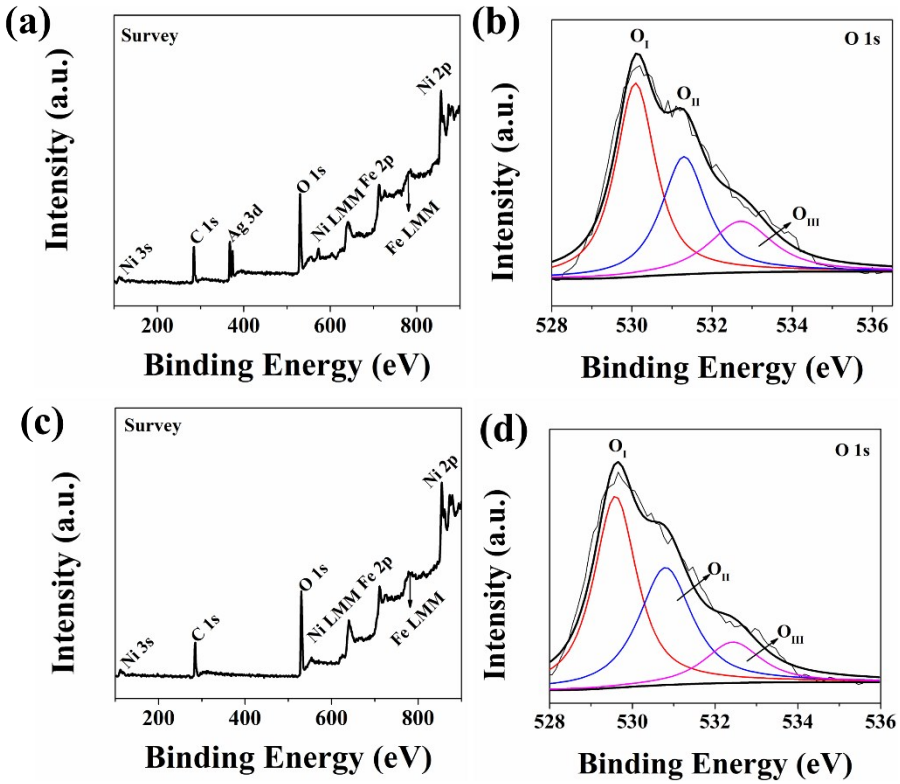

Fig. S9 XPS spectra of (a) Survey and (b) O 1s for NiFe-O/Ag (with Ag NWs); XPS spectra of (c) Survey and (d) O 1s for NiFe-O (without Ag NWs).

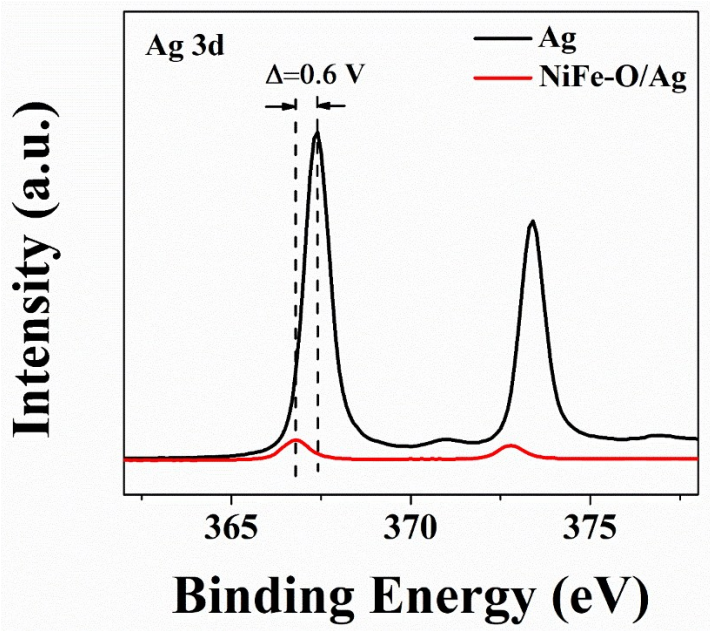

Fig. S10 XPS spectrum of Ag 3d for Ag NWs and NiFe-O/Ag (supported on NWs).

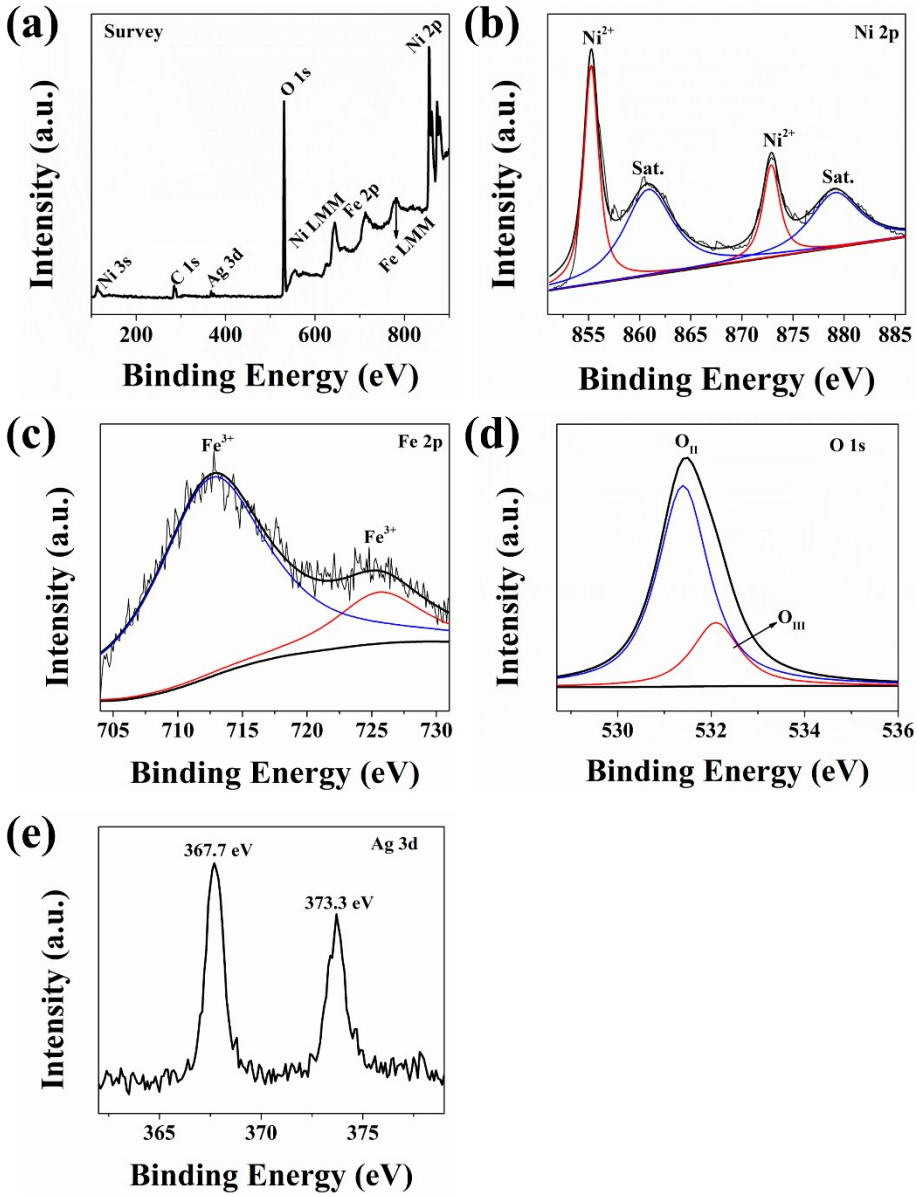

Fig. S11 XPS spectra of (a) survey, (b) Ni 2p, (c) Fe 2p, (d) O 1s and (e) Ag 3d for NiFe-LDH/Ag sample.

The survey XPS spectrum of NiFe-LDH/Ag sample signifies the presence of Ni, Fe, O, and Ag elements. (Fig. S11a) The XPS spectra of Ni 2p and Fe 2p show peaks for Ni^{2+} (855.3 and 872.9 eV) and Fe^{3+} (712.8, 726.1 eV) species (Fig. S11b and Fig.

S11c). Notably, the binding energies of Ni^{2+} and Fe^{3+} are nearly the same as those of NiFe-O without Ag NWs (i.e. Ni^{2+} centered at 855.3, and 873.2 eV; Fe^{3+} centered at 712.9 and 726.2 eV) (Fig. 2). In case of Ag 3d spectrum, the peaks at 367.7 and 373.3 eV for metallic Ag (Fig. S11e), which are similar with those for bare Ag NWs (367.5 and 373.4 eV). The above results undoubtedly suggest that there may be no electron transfer between NiFe-LDH and Ag NWs. The O 1s spectra display peaks of O_{II} (531.3 eV), and O_{III} (532.7 eV) for oxygen atoms of absorbed hydroxyl groups, and oxygen atoms of absorbed water, respectively. (Fig. S11d)

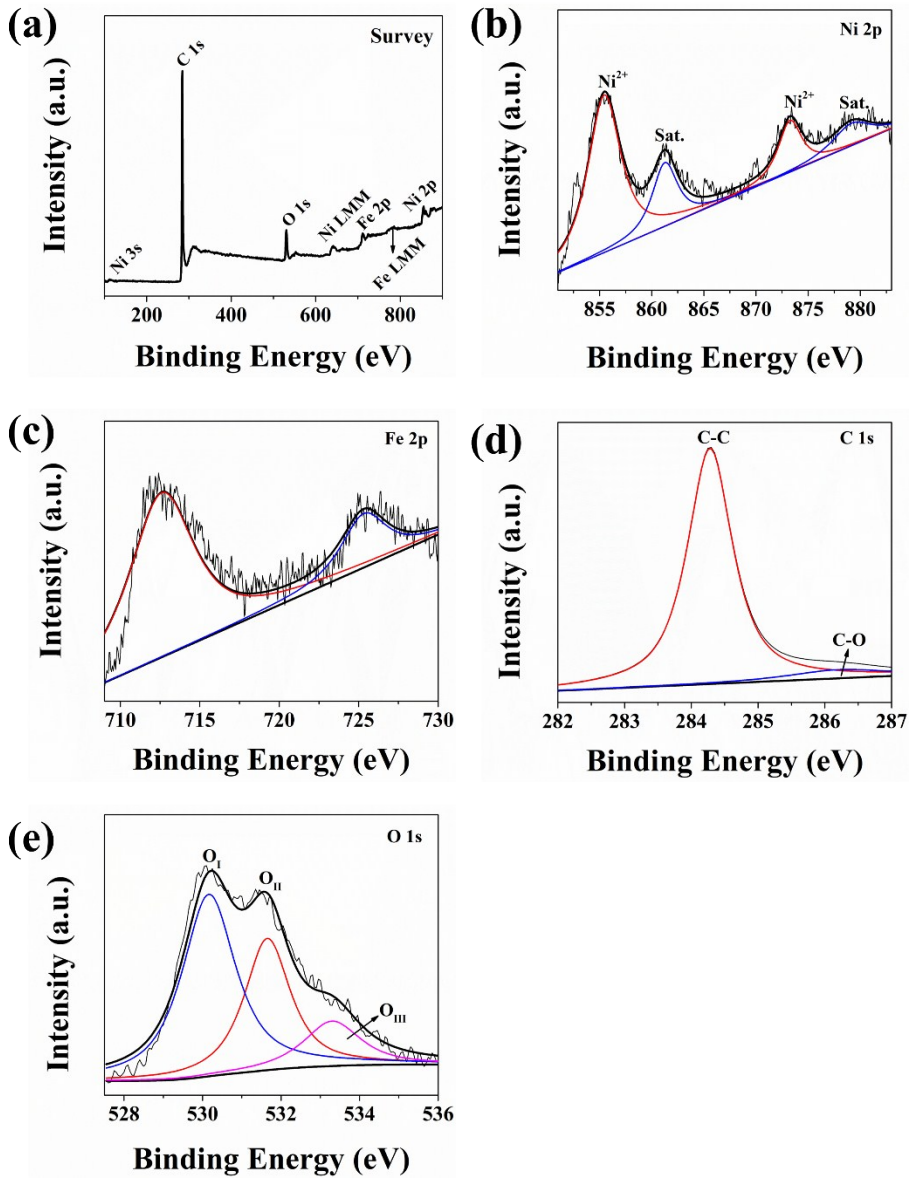

Fig. S12 XPS spectra of (a) survey, (b) Ni 2p, (c) Fe 2p, (d) C 1s and (e) O 1s for NiFe-O/CNT sample.

The survey XPS spectrum of NiFe-O/CNT sample indicates the presence of Ni, Fe, O, and C elements. (Fig. S12a) The Ni 2p spectrum shows peaks centered at 855.4 and 873.2 eV for Ni^{2+} species., whereas the Fe 2p spectrum displays peaks centered at 712.7 and 725.7 eV for Fe^{3+} species. (Fig. S12b and Fig. S12c) Indeed, those binding energies of Ni^{2+} and Fe^{3+} species are quite similar with those for NiFe-O without Ag NWs. Furthermore, the C1s spectrum indicates a distinct peak centered 284.6 eV for

graphitic carbon, and a tiny peak centered at 286.3 eV for C–O. (Fig. S12d) The above results indicate there may be no electron transfer between NiFe-O and CNT. Besides, O 1s spectra display peaks of O_I (530.1 eV), O_{II} (531.3 eV), and O_{III} (532.7 eV), corresponding to oxygen atoms bound to metals (i.e. Ni, and Fe), oxygen atoms of absorbed hydroxyl groups, and oxygen atoms of absorbed water. (Fig. S13e)

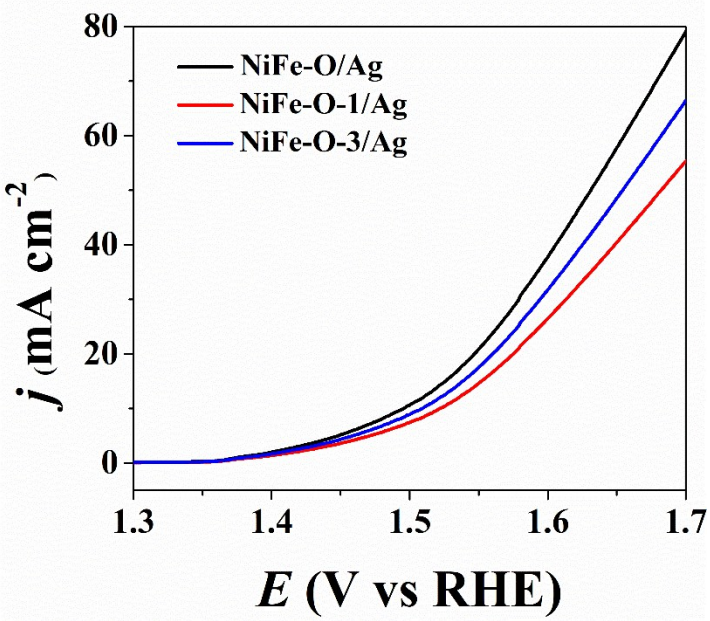

Fig.S13 LSV curves of NiFe-O/Ag, NiFe-O-1/Ag, and NiFe-O-3/Ag. The molar ratio of Ni^{2+} to Fe^{3+} ions for them are 2, 1, and 3.

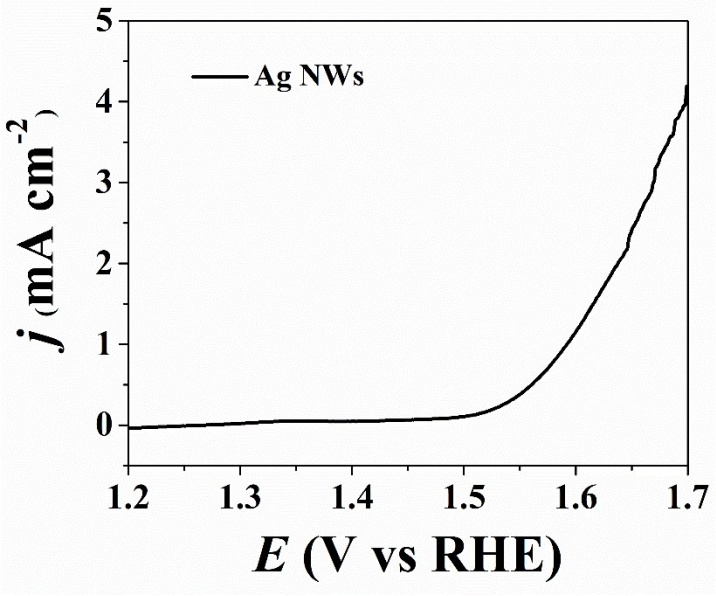

Fig. S14 LSV curve of bare Ag NWs for OER in 1 M KOH.

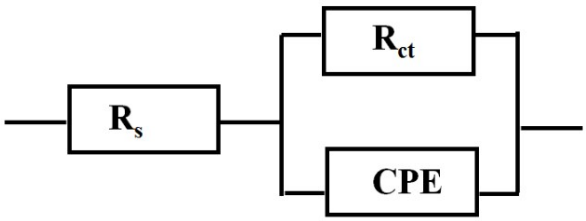

Fig. S15 Equivalent circuit diagrams of NiFe-LDH/Ag, NiFe-O/Ag, NiFe-O, and NiFe-O/CNT electrocatalysts for OER at the overpotential of 300 mV.

According to previous literatures[4, 5], the Nyquist plots in Fig. 3c are fitted by a model with one time constant (R_{ct}||CPE), which can be attributed to charge transfer resistance (R_{ct}). The fitted results are shown in Table S1.

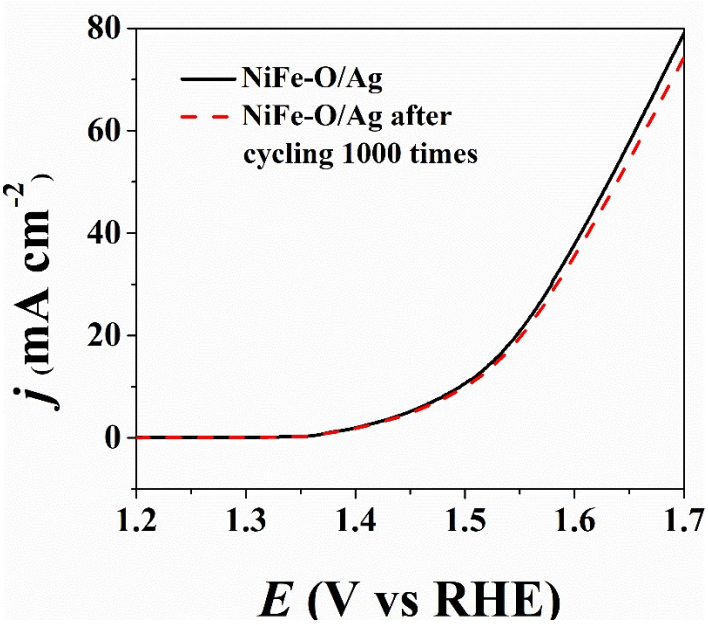

Fig. S16 LSV of NiFe-O/Ag before and after cycling 1000 times over a potential range of 1.2-1.7 V.

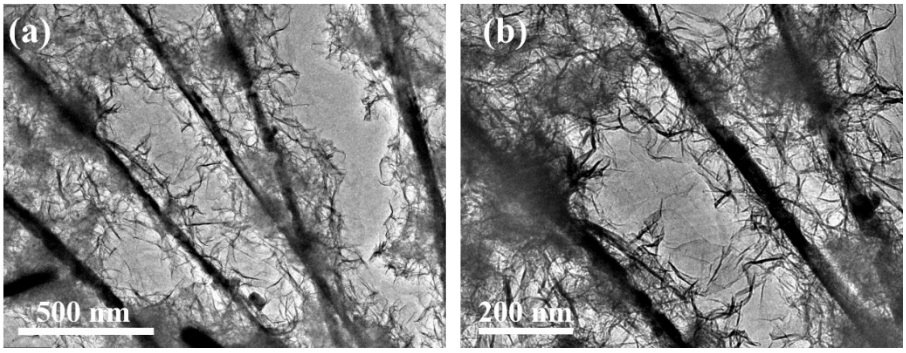

Fig. S17 TEM images of NiFe-O/Ag sample after stability test of 30 h.

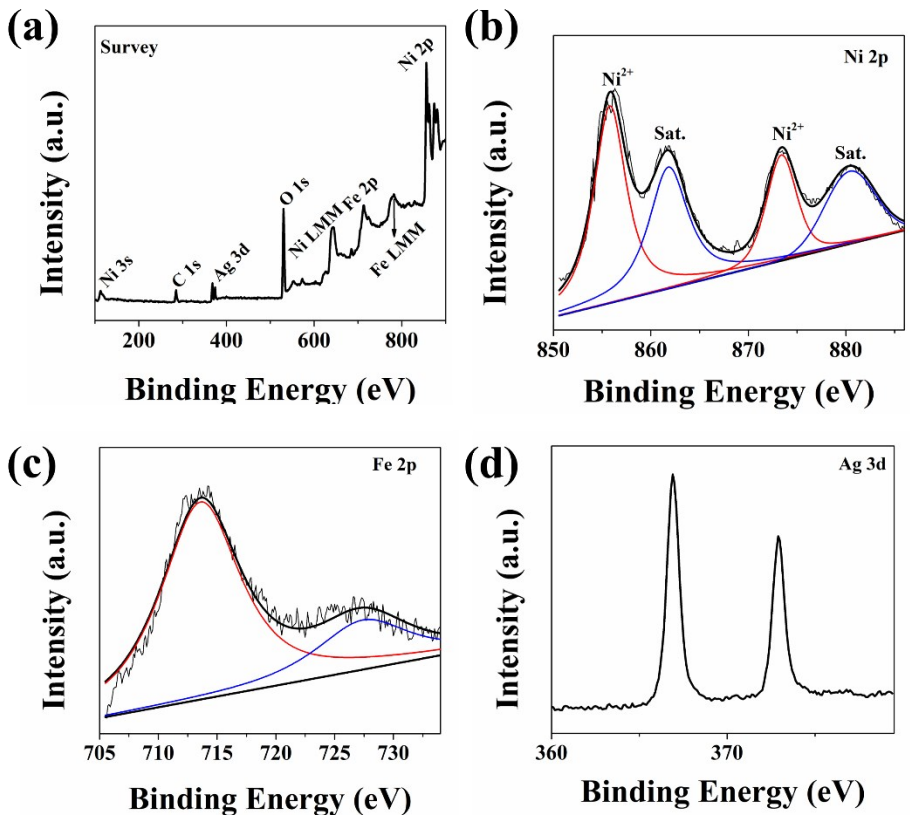

Fig. S18 XPS spectra of (a) survey, (b) Ni 2p, (c) Fe 2p, and (d) Ag 3d for NiFe-O/Ag after stability of 30 h

As shown in Fig. S18a, after stability test, the survey XPS spectrum of NiFe-O/Ag electrocatalyst signifies the presence of Ni, Fe, O, and Ag elements. The XPS spectrum of Ni 2p shows peaks centered at 855.9 and 873.5 eV for Ni^{2+} species. In case of Fe 2p, peaks centered at 713.8 and 727.5 eV for Fe^{3+} species. The XPS spectrum of Ag 3d display peaks centered at 366.9, 372.9 eV for metallic Ag. Notably, the above binding energies of Ni^{2+}, Fe^{3+}, and metallic Ag are quite similar to those for NiFe-O/Ag before stability test.

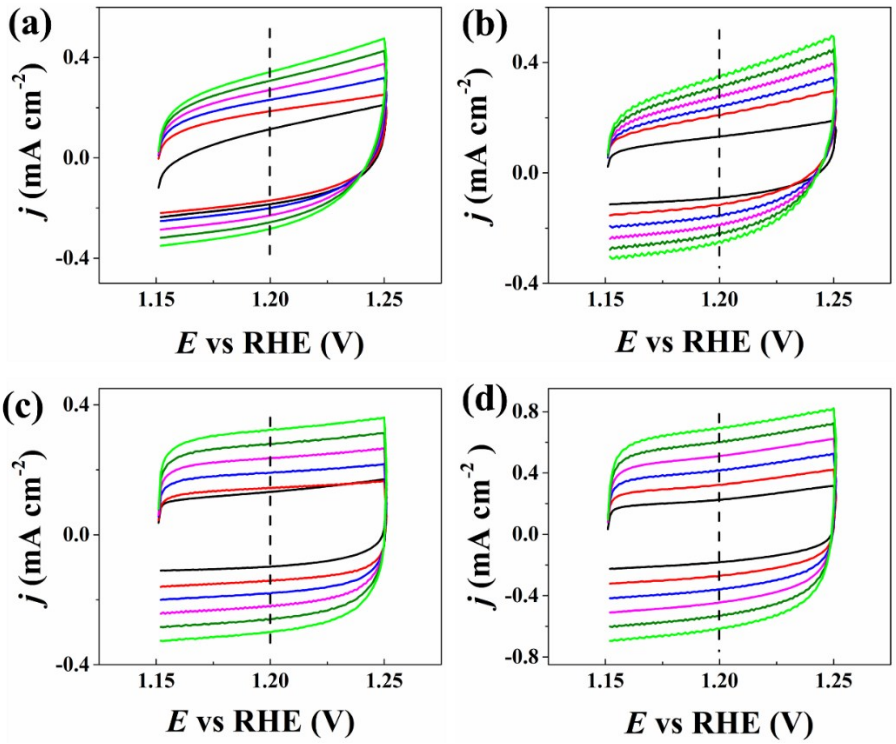

Fig. S19 Cyclic voltammetry curves of (a) NiFe-LDH/Ag, (b) NiFe-O, (c) NiFe-O/Ag, (d) NiFe-O/CNT at different scan rate from 40 to 140 mV s^{-1}.

Table S1 Comparison of NiFe-O/Ag with other non-noble-metal electrocatalysts reported in the literature for electrocatalytic OER performance in alkaline media

Catalyst	**Electrolyte**	**Loading (mg cm^{-2})**	**Overpotential (mV) at 10 mA cm^{-2}**	**Reference**
NiFe-O/Ag	1.0 M KOH	0.286	265	This work
NiCoFe-LDH/CFC	1.0 M KOH	0.45	280	6
$Fe_xCo_{1-x}OOH$ PNSAs/CFC	1.0 M KOH	1.03	266	7
NiFe/NiFeOx(y)	0.1 M KOH	0.25	340	8
E-CoFe LDHs	1.0 M KOH	0.204	302	9
$NiCo_2O_4$	1.0 M NaOH	-	320	10
NiFe LDH	1.0 M KOH	1.00	300	11
FeNi-LDH/Ti_3C_2-MXene	1.0 M KOH	0.2	298	12
$NiCoO_2$@CFP	0.1 M KOH	-	303	13
Ni_2Fe-SDS-LDH/CFP	1.0 M KOH	1.00	289	14
CoMn LDH	1.0 M KOH	0.142	324	15
α-$Ni(OH)_2$	0.1 M KOH	0.2	331	16
LDH/GSH	0.1 M KOH	0.25	350	17
nNiFe LDH/NGF	0.1 M KOH	0.25	337	18
$Fe(TCNQ)_2$/Fe	1.0 M KOH	0.49	340	19
CP@FeP	1.0 M KOH	0.7	350	20
NiFeS-2	0.1 M KOH	0.25	286	21
CoO/CoFe LDHs	1.0 M KOH	0.2	254	22
NiCdFe	0.1 M NaOH	-	290	23
$Ni_{0.75}Fe_{0.25}Se_2$	1.0 M KOH	0.255	267	24

NiFe@CN-G	1.0 M KOH	0.286	320	25

Table S2 Circuit parameters extracted from Fig. 3c for NiFe-LDH/Ag, NiFe-O/Ag, NiFe-O, and NiFe-O/CNT electrocatalysts.

Samples	**R_s (Ω)**	**R_{ct} (Ω)**	**CPE-T (S*s^CPE-P)**	**CPE-P**
NiFe-LDH/Ag	1.7	3.6	0.039	0.64
NiFe-O/Ag	1.8	3.5	0.054	0.63
NiFe-O	1.5	17.9	0.013	0.80
NiFe-O/CNT	1.8	4.3	0.025	0.77

Table S3 Characteristics of as-synthesized electrocatalysts (i.e. NiFe-LDH/Ag, NiFe-O/Ag, NiFe-O, and NiFe-O/CNT)

Catalysts	**Overpotential (mV) at 10 mA cm^{-2}**	**Tafel slope (mV/dec)**	**C_{dl} (mF cm^{-2})**	**ECSA (cm^2)**
NiFe-LDH/Ag	310	121.6	3.3	82.5
NiFe-O/Ag	265	38.0	4.0	100.0
NiFe-O	360	96.7	3.7	92.8
NiFe-O/CNT	320	103.0	4.5	113.3

References:

1. J. Jiu, T. Araki, J. Wang, M. Nogi, T. Sugahara, S. Nagao, H. Koga, K. Suganuma, E. Nakazawa, M. Hara, H. Uchida and K. Shinozaki, *J. Mater. Chem. A,* 2014, **2**, 6326-6330.

2. C. C. McCrory, S. Jung, J. C. Peters and T. F. Jaramillo, *J. Am. Chem. Soc.,* 2013, **135**, 16977-16987.

3 S. Anantharaj, K. Karthick, M. Venkatesh, T. V. S.V. Simha, A. S. Salunke, L. Ma, H. Liang, S. Kundu, *Nano Energy,* 2017, **39**, 30-43.

4 J. Xie, H. Zhang, S. Li, R. Wang, X. Sun, M. Zhou, J. Zhou, X.W. Lou, Y. Xie, *Adv. Mater*., 2013, **25**, 5807–5813.

5 Q. Hu, X. Liu, B. Zhu, L. Fan, X. Chai, Q. Zhang, J. Liu, C. He, Z. Lin, *Nano Energy,* 2018, **50**, 212-219.

6. T. Wang, W. Xu and H. Wang, *Electrochimica Acta,* 2017**, 257**, 118-127.

7. S. H. Ye, Z. X. Shi, J. X. Feng, Y. X. Tong and G. R. Li, *Angew. Chem. Int. Edit.,* 2018**, 57**, 2672-2676.

8. K. Zhu, M. Li, X. Li, X. Zhu, J. Wang and W. Yang, *Chem. Commun.,* 2016**, 52**, 11803-11806.

9. P. Zhou, Y. Wang, C. Xie, C. Chen, H. Liu, R. Chen, J. Huo and S. Wang, *Chem. Commun.,* 2017, **53**, 11778-11781.

10. Chen. R, Wang. H. -Y., Miao. J, Yang. H and Liu. B, *Nano Energy,* 2015**, 11**, 333-340.

11. Song. F and Hu. X, *Nat. Commun.,* 2014**, 5**, 4477.

12. M. Yu, S. Zhou, Z. Wang, J. Zhao and J. Qiu, *Nano Energy,* 2018,**44**,181-190.

13. Y. Yang, M. Zhou, W. Guo, X. Cui, Y. Li, F. Liu, P. Xiao and Y. Zhang, *Electrochimica Acta,* 2015, **174**, 246-253.

14. H. Zhong, X. Cheng, H. Xu, L. Li, D. Li, P. Tang, N. Alonso-Vante and Y. Feng, *Electrochimica Acta,* 2017, **258**, 554-560.

15. F. Song and Hu. X, *J. Am. Chem. Soc.,* 2014**, 136**, 16481-16484.

16. M. Gao, W. Sheng, Z. Zhuang, Q. Fang, S. Gu, J. Jiang and Y. Yan, *J. Am. Chem. Soc.,* 2014**, 136**, 7077-7084.

17. X. Zhu, C. Tang, H. -F.Wang, Q. Zhang, C. Yang and F. Wei, *J. Mater. Chem. A,*

2015**, 3**, 24540-24546.

18. C. Tang, H. S. Wang, H. F. Wang, Q. Zhang, G. L. Tian, J. Q. Nie and F. Wei, *Adv Mater.,* 2015, **27**, 4516-4522.

19. M. Xie, X. Xiong, L. Yang, X. Shi, A. M. Asiri and X. Sun, *Chem. Commun.,* 2018**, 54**, 2300-2303.

20. D. Xiong, X. Wang, W. Li and L. Liu, *Chem. Commun.,* 2016**, 52**, 8711-8714.

21. B. Q. Li, S. Y. Zhang, C. Tang, X. Cui and Q. Zhang, *Small,* 2017**, 13**, 1700610.

22. Z. W. Gao, T. Ma, X. M. Chen, H. Liu, L. Cui, S. Z. Qiao, J. Yang and X. W. Du, *Small,* 2018, DOI: 10.1002/smll.201800195.

23. J. -H. Kim, D. H. Youn, K. Kawashima, J. Lin, H. Lim and C. B. Mullins, *Appl. Catal. B: Environ.,* 2018, **225**, 1-7.

24. L. Lv, Z. Li, K. -H. Xue, Y. Ruan, X. Ao, H. Wan, X. Miao, B. Zhang, J. Jiang, C. Wang and K. Ostrikov, *Nano Energy,* 2018, **47**, 275-284.

25. C. Deng, K. -H. Wu, J. Scott, S. Zhu, R. Amal and D.-W. Wang, *ChemElectroChem,* 2018, **5**, 732-736.